Chapter 3

Characterization Techniques

3.1 Introduction

In material science, different instruments are used to study materials and understand their properties. In this work, X-ray diffraction and UV-Visible spectroscopy have been used for characterization and study of properties of the synthesized samples.

3.2 X- Ray Diffraction (XRD)

X-ray diffraction is a nondestructive technique to determine crystal structure of metals, alloys, minerals, inorganic compounds, polymer and organic materials and to derive information such as crystallite size, lattice-strain, crystalline phase and orientation.

3.2.1 Fundamental Principles of X-ray Diffraction

X-rays, a form of electromagnetic radiation with shorter wavelengths, are generated within a cathode ray tube through a process initiated by heating of a filament to emit electrons. These emitted electrons are then accelerated by applying voltage and directed towards a target material. Upon collision with the target material, electrons with sufficient energy can displace inner shell electrons, resulting in the emission of characteristic X-rays. Besides, continuous X-rays are also generated.

These emitted X-rays encompass various components, with the most prevalent ones being the K_α and K_β lines. The specific wavelength of these characteristic X-rays is contingent upon the choice of target material, such as Copper (Cu), Iron (Fe), Molybdenum (Mo) or Chromium (Cr). Notably, Copper is the most utilized target material for powder diffraction purposes.

In the case of copper, the characteristic wavelength of the Kα line is precisely measured to be 1.5418 angstroms (Å), which serves as a pivotal parameter in X-ray diffraction analyses **[1]**.

In 1912, Max von Laue made a groundbreaking revelation: crystalline substances exhibit a remarkable property when subjected to X-rays, essentially functioning as a diffraction grating due to the X-rays' wavelengths aligning with the interatomic distances within crystals. Consequently, when X-rays interact with these crystalline structures, they undergo diffraction, resulting in a phenomenon where the diffracted X-rays either

reinforce each other (constructive interference) or cancel each other out (destructive interference).

This constructive interference occurs under specific geometric conditions, facilitating the emergence of a distinct pattern of diffracted X-rays. It's crucial to note that X-ray diffraction operates on the principle of elastic scattering, signifying that the redirection of the X-ray waves' motion transpires without any loss of energy. This principle underscores the precision and accuracy of X-ray diffraction analyses, enabling researchers to glean valuable insights into the atomic arrangement and structural properties of crystalline materials.

Crystals exhibit a distinctive atomic arrangement, characterized by regular spacing between atoms. This spatial arrangement effectively serves as a series of grating lines for diffraction. When X-rays interact with these atomic lattices, the waves scattered by individual atoms can interfere with each other. If the scattered waves are in phase, they undergo constructive interference, resulting in the emergence of a diffracted beam in a specific direction.

The direction of this diffracted beam is intricately linked to both the wavelength of the incident X-rays and the inherent properties of the crystalline material. This relationship between the wavelength of X-rays and the spacing of the atomic planes was elucidated by W. L. Bragg in 1913. Bragg's formulation provides a fundamental understanding of how X-rays interact with crystalline structures, paving the way for the development of X-ray diffraction as a powerful analytical technique in the field of materials science **[2]**. A pattern of scattered X-rays or the diffraction pattern is mathematically related to the structural arrangement of atoms causing the scattering.

In the depicted arrangement of atoms shown in Figure 1, each atomic plane reflects the incident wave. When an X-ray beam with a wavelength of λ strikes a crystal plane at an angle θ, the resulting diffracted wave mirrors the incident wave's angle relative to the atomic plane. The mathematical relation is given by,

$$n\lambda = 2d\ sin\theta$$

where d is the spacing between atomic planes, which is a characteristic of the material.

This equation is known as Bragg's Law. By varying the angle θ, the Bragg's Law conditions are satisfied by different d – spacing in polycrystalline materials.

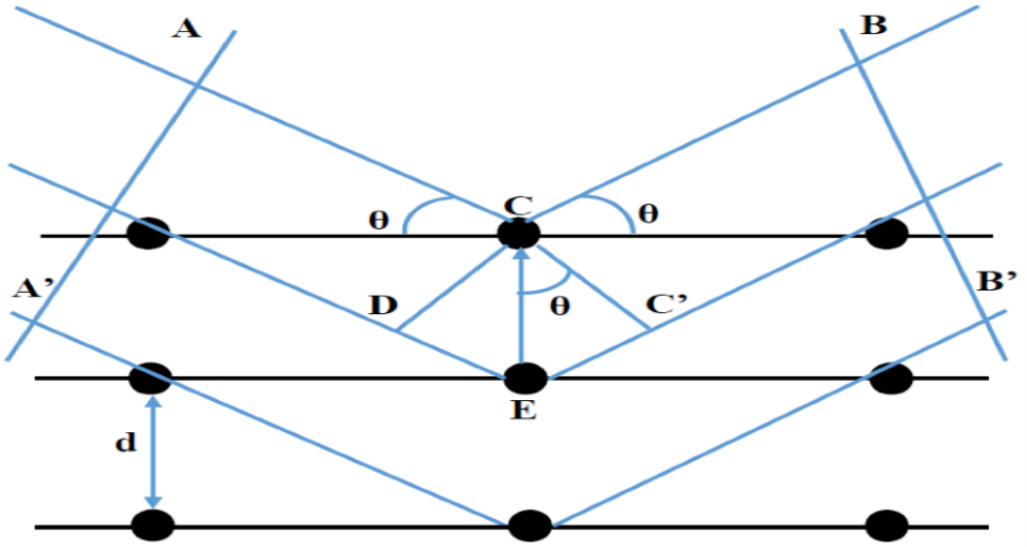

Figure1: Diffraction of X-rays by crystal.

3.2.2 Instrumentation for X-ray diffraction

The essential components of an X-ray diffractometer include the X-ray source, detector, and assembly, all positioned along the circumference of a circular arc. Figure 2 illustrates the geometric setup of an X-ray diffractometer, where the angle between the specimen plane and the X-ray source is denoted as θ. The angle between the projection of the X-ray source and the detector is labelled as 2θ. This configuration produces what is known as a θ-2θ scan X-ray diffraction pattern.

In the θ-2θ geometry, the X-ray source remains fixed while the detector traverses a range of angles. The measurement range for 2θ typically extends from 0° to 170°, although this can vary depending on the crystal structure of the material under investigation. This setup is widely employed due to its versatility and effectiveness in analysing crystal structures.

Another useful configuration is the θ-θ geometry, where both the X-ray source and the detector move in opposite directions within a vertical plane centred above the specimen. This alternative geometry offers distinct advantages in certain experimental scenarios.

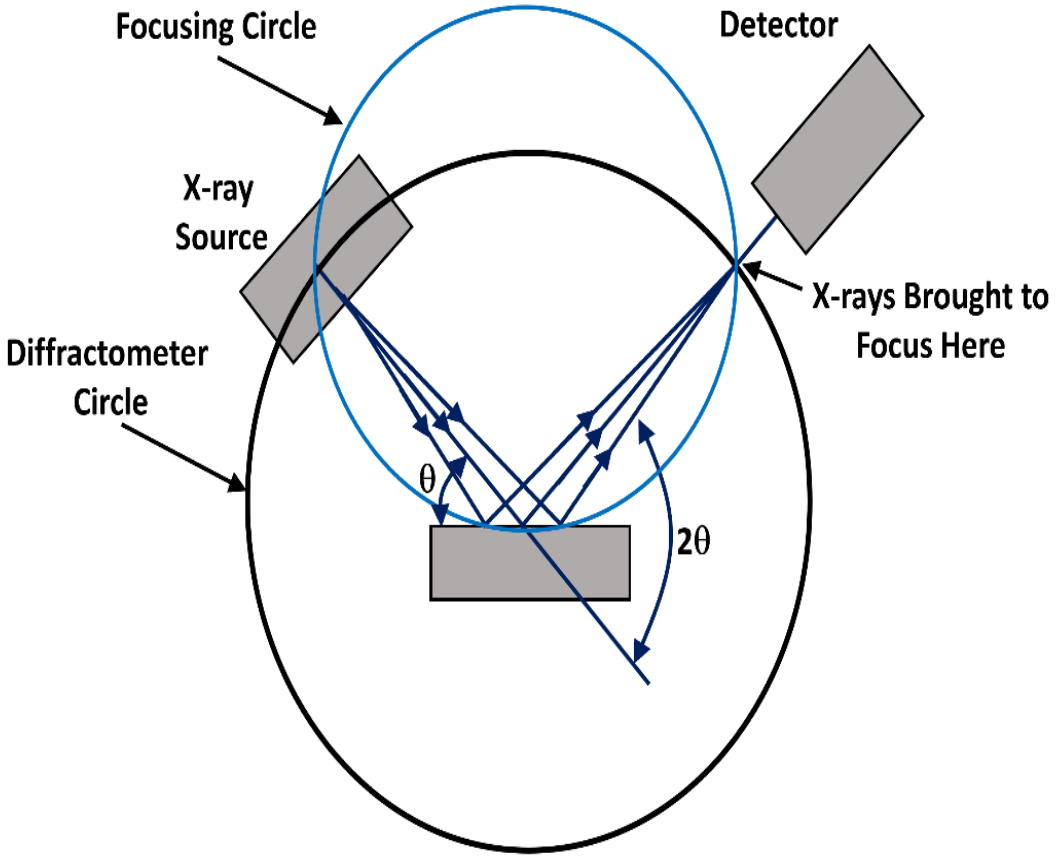

Figure 2: Geometry of an X-ray Diffractometer **[2]**.

In the θ-2θ geometry, the X-ray source remains fixed while the detector traverses a range of angles. The measurement range for 2θ typically extends from 0° to 170°, although this can vary depending on the crystal structure of the material under investigation. This setup is widely employed due to its versatility and effectiveness in analysing crystal structures.

Another useful configuration is the θ-θ geometry, where both the X-ray source and the detector move in opposite directions within a vertical plane centred above the specimen. This alternative geometry offers distinct advantages in certain experimental scenarios.

The circular path formed by the X-ray source, detector, and specimen is commonly referred to as the goniometer circle. This circular arrangement ensures precise positioning and alignment of the components, enabling accurate measurements and analysis during X-ray diffraction experiments.

3.2.3 X-ray diffraction pattern

The X-ray diffraction pattern comprises multiple peaks, often referred to as reflections, plotted against the diffraction angle (2θ). Each reflection corresponds to X-rays diffracted from specific planes within a crystal. The intensity of these peaks correlates with the number of X-ray photons of a particular energy detected by the apparatus.

The position of these peaks in the X-ray diffraction pattern is intricately tied to the crystal structure of the material being analysed. Furthermore, the number of peaks is influenced by the symmetry of the crystal structure, with reduced symmetry resulting in an increased number of diffraction peaks.

The 2θ value of each peak provides valuable insights into the orientation and positioning of specific crystal planes within the material. Additionally, the width of individual peaks, often denoted by the full width at half the maximum (FWHM), can offer information regarding crystallite size and the presence of lattice distortions (strain) within the crystal lattice.

Powder diffraction data for various crystals is compiled by the Joint Committee on Powder Diffraction Standards (JCPDS). This database contains an extensive collection of single-phase X-ray powder diffraction patterns, presented in the form of tables detailing interplanar spacing (d) and corresponding relative intensities. With over 100,000 patterns available, this resource serves as a comprehensive reference for researchers.

X-ray diffraction is primarily utilized for identifying unknown crystalline materials. Moreover, it enables the evaluation of various structural parameters and information from the diffraction pattern. These parameters include crystallite size, phase composition, dislocation density, preferred orientation of different crystal planes, lattice strain, and lattice parameters, among others.

Crystallite Size

The Scherrer equation, attributed to Scherrer, provides a means to determine the size of crystallites within a solid by correlating it with the broadening of peaks observed

in its diffraction pattern **[3]**. This fundamental equation serves as a valuable tool in materials science and crystallography for estimating the dimensions of crystalline domains.

$$d = \frac{K\lambda}{\beta\cos\theta}$$

where,

d = crystallite size

K = dimensionless shape factor

λ = wavelength of X-ray used

β = line broadening at half the maximum intensity (FWHM), after subtracting the instrumental line broadening in (radians)

θ = Bragg diffraction angle

The Scherrer equation is limited to nano scale crystallites.

Phase Composition

The composition of different phases within a material can be deduced from the X-ray diffraction pattern. For instance, in the case of two distinct phases of TiO_2, namely Anatase and Rutile coexisting within the material, the proportion of one phase (Rutile) can be determined using the following relationship **[4]**.

$$X_R = \left[1 + 1.26\left(\frac{I_A}{I_R}\right)\right]^{-1}$$

Where,

X_R = the mass fraction of Rutile

I_A = the intensity of the highest peak for Anatase

I_R =the intensity of the highest peak for Rutile.

Lattice Strain

In present work, the lattice strain has been calculated using the relation **[5]**.

$$\eta = \left[\frac{\lambda}{t\ cos\theta} - \frac{\beta\ \pi}{180}\right]\frac{1}{\tan\theta}$$

where,

t = grain size

λ = wavelength of X-ray

β = full width at half maximum of the diffraction peak

θ = angle of diffraction.

Crystallinity Index

The concept of the crystallinity index serves to quantify the relative abundance of the crystalline component within a material. This index can be computed utilizing the following equation **[6]**.

$$CI = \frac{I_{max} - I_{min}}{I_{max}}$$

$$CI = \left(\frac{I_{max} - I_{min}}{I_{max}}\right) \times 100\%$$

where,

I_{max} = height of the highest peak

I_{min} = height of the minimum of the highest peak

Lattice Parameters

To determine the lattice parameters 'a' and 'c' for a tetragonal crystal structure, one can employ the following method: **[7]**.

$$\frac{1}{d^2} = \frac{(h^2 + k^2)}{a^2} + \frac{l^2}{c^2}$$

where,

d = inter planar spacing determined using Bragg's equation

h, k, l = the miller indices of the lattice plane.

3.3 UV-Visible Spectroscopy

3.3.1 Introduction

UV-Visible absorption spectroscopy, also known as absorption or reflectance spectroscopy, serves as a vital tool for examining the optical properties of materials. In this technique, molecules absorb specific wavelengths within the electromagnetic spectrum, leading to electronic transitions. UV-Visible spectroscopy involves subjecting the material to ultraviolet and visible radiation, typically ranging from 200 nm to 900 nm in wavelength.

At its core, UV-Visible spectroscopy operates on the principle of electronic transitions. The valence electron in a molecule resides within one of three types of electron orbitals: σ-bonding (associated with single bonds), π-bonding (related to multiple bonds), and non-bonding (corresponding to lone pair electrons). The π-electrons or nonbonding electrons within molecules transition to higher anti-bonding molecular orbitals upon absorbing energy from ultraviolet or visible light **[8]**.

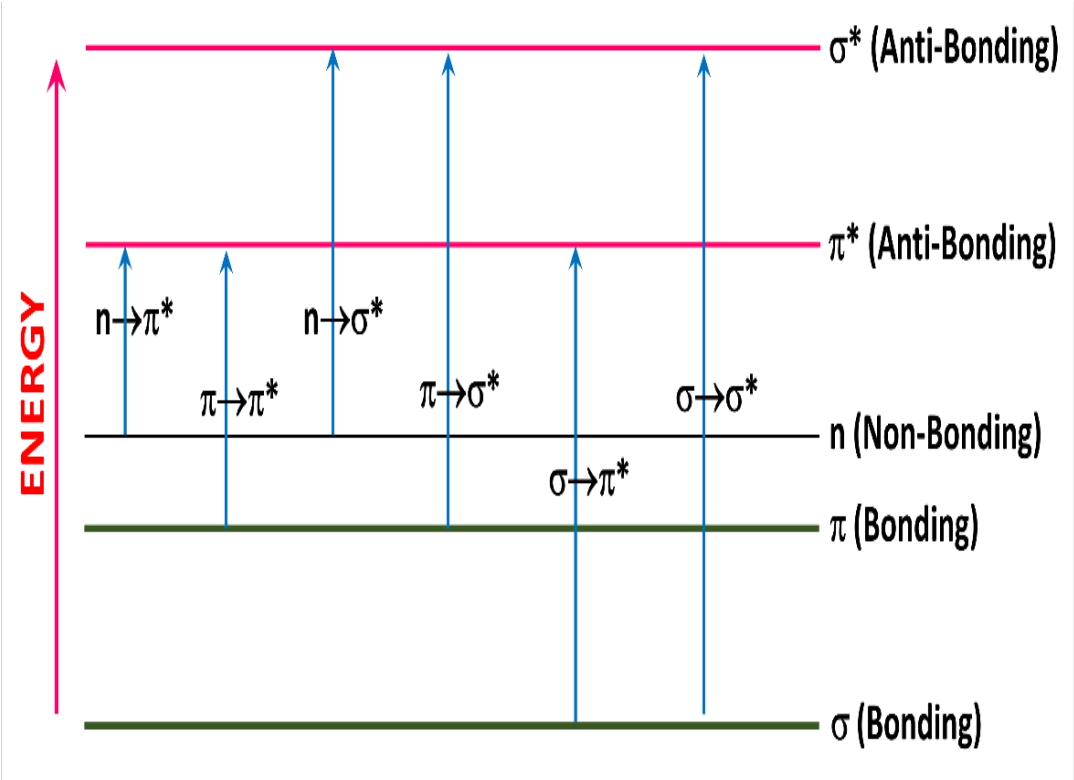

Figure 3: Different transitions between the bonding and anti-bonding electronic states **[9]**.

In UV-Visible spectroscopy, the majority of absorption events stem from transitions involving π-bond electrons and non-bonding electrons. Here's a breakdown of their characteristics and their role in absorption:

σ-bond electrons: These electrons occupy the lowest energy levels and are inherently stable. Their transition to higher energy states necessitates significant energy input, typically in the form of lower wavelengths of ultraviolet radiation.

π-bond electrons: Comparatively, π-bond electrons possess higher energy levels than σ-bond electrons, rendering them relatively less stable. As a result, they require less energy to transition to higher energy states and thus absorb ultraviolet and visible radiation.

Non-bonding electrons: Non-bonding electrons exhibit energy levels even higher than those of π-electrons and σ-electrons. They are readily excited by ultraviolet or visible radiation, making them susceptible to absorption events **[10, 11]**. In Figure 3, various transitions between bonding and anti-bonding electronic states are depicted.

3.3.2 The UV-Visible Spectrometer

The instrument utilized for UV-Visible spectroscopy is known as a UV-Visible spectrometer. Its operation is based on the Lambert-Beer Law. This fundamental law states that the absorbance of a sample at a specific wavelength is directly proportional to the molar absorptivity of the substance, the path length, and the concentration of the absorbing substance. Mathematically, this relationship is expressed as:

$$A = \varepsilon \cdot l \cdot c$$

where:

A = measured absorbance,

ε = the molar absorptivity of the substance (a constant at each wavelength),

l = path length, and

c = concentration of the substance.

Experimental measurements are typically conducted in terms of transmittance (T). The spectrometer assesses the intensity (I) of light passing through the sample and contrasts it with the intensity of incident light (I_0) on the sample. The transmittance (T) is then determined as the ratio of I/I_0. The relationship between absorbance (A) and transmittance (T) is defined by:

$$A = -\log(T) = -\log\left(\frac{I}{I_o}\right)$$

Furthermore, the UV-Visible spectrometer can be configured to measure reflectance. In this scenario, the instrument evaluates the intensity of light reflected from a sample (I) and compares it to the intensity of light reflected from a reference material (I_0). The ratio $I/I_0$is referred to as reflectance.

The UV-Visible Spectrometer is composed of four fundamental components.

Light Source: The spectrometer necessitates a light source capable of emitting the entire visible spectrum alongside near-ultraviolet radiation. Typically, a combination of lamps is employed for this purpose. A deuterium lamp provides the UV portion of the spectrum, while tungsten or halogen lamps cater to the visible segment. Alternatively, Xenon arc lamps, offering continuous emission from 160 to 900 nm, can be utilized. More recently, light-emitting diodes (LEDs) have also been incorporated for visible wavelengths **[12]**.

Monochromator: Traditionally, the monochromator comprises a prism, though modern implementations favour gratings over prisms. The monochromator's role is to isolate specific wavelengths of light for analysis.

Detector: The detector, typically a photomultiplier tube or photodiode, captures and measures the intensity of light transmitted through the sample.

Sample Holder: Commonly referred to as a cuvette or cell, the sample holder accommodates the substance under analysis. It is typically constructed from glass or quartz. The cuvette contains a dilute solution of the test substance, with the solvent carefully selected to minimize its own absorption of light within the wavelength range of 200 to 900 nm. Various solvents and their corresponding absorption wavelengths are detailed in Table 1.

Table 1: Different solvents and their minimum absorption wavelengths**.**

Solvent	Minimum Wavelength (nm)
Ethanenitrile	**190**
Water	**191**
Cyclohexane	**195**
Hexane	**201**
Methanol	**203**
Ethanol	**204**
Ethoxyethane	**215**
Dichloromethane	**220**
Trichloromethane	**237**
Tetrachloromethane	**257**

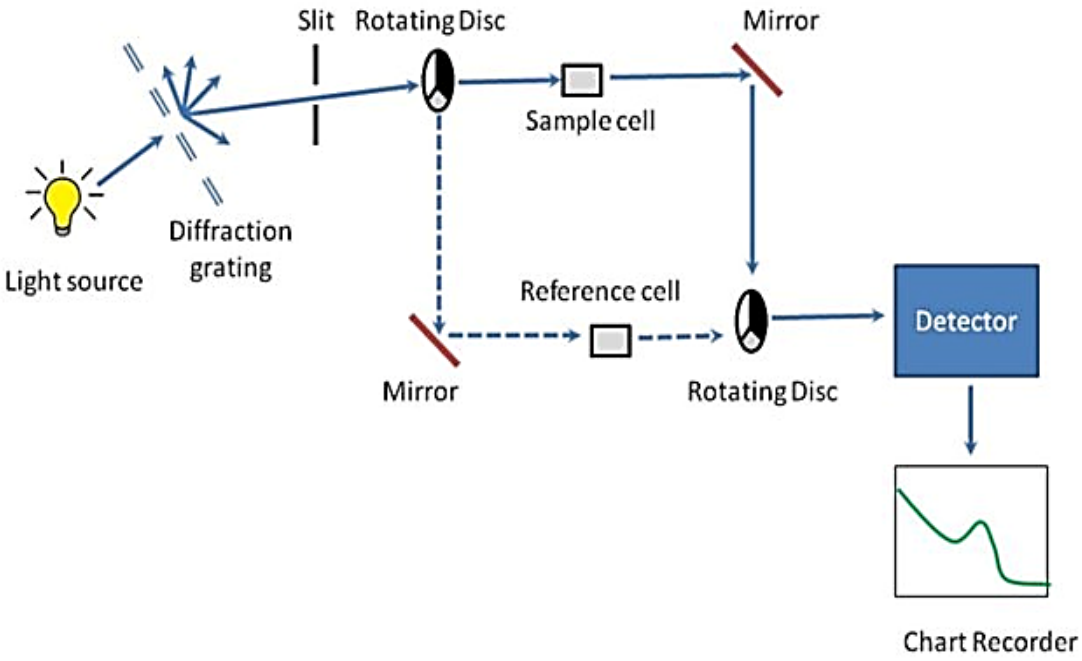

Figure 4: Schematic diagram of UV-Visible Spectrometer **[13]**.

In the dual-beam UV-Visible spectrometer, illustrated in Figure 4, the operational mechanism is straightforward. Initially, a beam of light is dispersed into its constituent wavelengths using a diffraction grating. The resultant monochromatic beam encounters a rotating disc comprising three distinct segments: a black section, a mirrored section, and a transparent section.

When the monochromatic light strikes the transparent section of the rotating disc, it traverses directly through the sample cell. Subsequently, the light is redirected towards a second rotating disc via a mirror. The rotation of this second disc is synchronized such that upon arrival of light from the first disc, it intersects with the mirrored section. This causes the light to bounce off towards the detector.

Alternatively, if the monochromatic beam encounters the mirrored section of the first rotating disc, it is reflected downward along the green path. Here, the light passes through a reference cell before reaching the second disc. Upon reaching this second disc, the light intersects with the transparent section, allowing it to proceed directly to the detector.

In the event that the monochromatic light encounters the black section of the first rotating disc, it is obstructed, temporarily halting the passage of light through the spectrometer. This pause enables the computer to adjust for any current generated by the detector in the absence of light, ensuring accurate measurements.

3.3.3 Applications of UV-Visible Spectrometer

UV-Visible spectroscopy serves as a pivotal technique for investigating the optical properties of various materials, with extensive applications in physics and chemistry. Its versatility is evident in several key areas.

Concentration Determination: A fundamental application involves determining the concentration of chromophores within a sample.

Compound Identification: UV-Visible spectroscopy aids in identifying organic compounds by comparing spectral peaks with known patterns, offering insights into structural features.

Impurity Detection: The technique facilitates the detection of impurities in materials and the identification of different functional groups.

Thin Film Characterization: UV-Visible spectroscopy enables the study of thin film properties such as reflectance, transmittance, and film thickness. Various methods have been developed for precise thickness measurement using this technique.

Bandgap Determination: Jan Tauc's relation enables the calculation of the optical bandgap of materials based on UV-Visible absorption spectra, offering insights into their electronic properties.

Optical Constants: UV-Visible spectroscopy provides valuable data on optical constants including refractive index, extinction coefficient, absorption coefficient, optical conductivity, and dielectric constants.

Overall, UV-Visible spectroscopy plays a crucial role in elucidating the optical behaviour and characteristics of materials, making it an indispensable tool in scientific research and industrial applications.

Absorption Co-efficient (α cm^{-1})

The absorption coefficient is a crucial parameter governing the amount of light or photons absorbed within a material, thereby influencing its optical properties. This essential parameter can be determined using the following formula:

$$\alpha = 2.303 \times \frac{\text{Absorbance}}{t}$$

where, t = path length (thickness of the film or thickness of the sample holder)

Extinction Coefficient (K)

The extinction coefficient, also referred to as the absorption index, quantifies the fraction of light lost due to scattering and absorption per unit distance travelled through the medium. This coefficient serves as a metric for gauging the material's effectiveness in scattering and absorbing electromagnetic radiation. A lower extinction coefficient indicates that the material permits electromagnetic waves to traverse with minimal obstruction **[8]**.

Expressed mathematically, the formula for the extinction coefficient is as follows:

$$K = \frac{\alpha\lambda}{4\pi}$$

Where, α = absorption co efficient

λ = absorbed wavelength

Optical Bandgap (E_g eV)

The bandgap represents the energy difference between the highest energy level in the valence band and the lowest energy level in the conduction band of a material. It's important to note that there are two distinct types of bandgaps: optical and electrical.

The optical bandgap pertains to the energy required to generate an exciton—a bound electron-hole pair—within the material, without necessarily separating the electron and hole. In contrast, the electrical bandgap encompasses both the energy needed to create an electron-hole pair and the subsequent energy required to separate them. Generally, optical conductivity is slightly lower than electrical conductivity due to these distinctions in bandgap properties.

Jan Tauc introduced a relation, commonly known as Tauc's relation, which provides a means to determine the optical bandgap of a material. This relation serves as a valuable tool in characterizing the optical properties and electronic structure of various materials.

$$\alpha = A(h\nu - Eg)^{\left(\frac{1}{n}\right)}$$

where,

A = constant

hν = photon energy

n = constant which depends on the type of transition

= 1/2 for direct allowed transitions

= 2 for indirect allowed transitions

= 3/2 for direct forbidden transitions

= 3 for indirect forbidden transitions

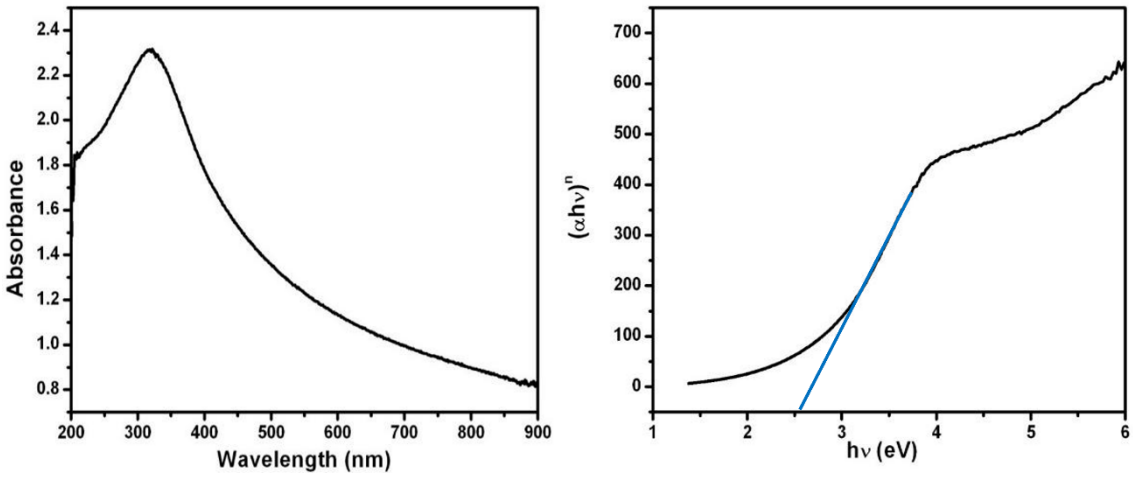

Figure 5: Absorption spectra and their corresponding Tauc's Plot.

To ascertain the optical bandgap of a material, the absorption spectrum is obtained. From this spectrum, the absorption coefficient (α) can be calculated. Subsequently, a plot of $(\alpha h\nu)^n$ versus hν is constructed, commonly referred to as Tauc's plot.

In Tauc's plot, the data points are typically plotted and analysed to identify a linear region. This linear region corresponds to the band-to-band transitions. Extrapolating this linear region to intersect the x-axis yields the bandgap energy, as shown in Figure 5.

Refractive Index (η)

V. Kumar and J. K. Singh have proposed a method to determine the refractive index of thin films or powdered materials using UV-Visible absorption spectra. This relation offers a means to quantify how much the speed of light is reduced within the medium, providing insights into the material's optical properties **[14]**.

$$\eta = KE_g^C$$

Where,

η = refractive index

E_g = bandgap

K = constant = 3.3668

C = constant = - 0.32234

Optical Conductivity (σ)

Optical conductivity, a fundamental material characteristic, refers to the electrical conductivity observed under the influence of an alternating electromagnetic field across the entire frequency spectrum, extending beyond just the visible region. This conductivity parameter encapsulates the material's response to electromagnetic radiation across various frequencies **[15].**

Expressed mathematically, the formula for optical conductivity is as follows:

$$\sigma = \frac{\alpha \eta c}{4\pi}$$

Where,

c = velocity of light

α = absorption co efficient

η = refractive index

References:

1. Härtwig, J., Hölzer, G., Förster, E., Goetz, K., Wokulska, K., & Wolf, J. (1994). Remeasurement of characteristic x-ray emission lines and their application to line profile analysis and lattice parameter determination. *Physica Status Solidi (a), 143*(1), 23-34.
2. Suryanarayana, C., & Norton, M. G. (1998). *X-ray diffraction: A practical approach*. Springer Science+Business Media.
3. Khalid, N. R., Ahmed, E., Hong, Z., Ahmad, M., Zhang, Y., & Khalid, S. (2013). Cu-doped TiO2 nanoparticles/graphene composites for efficient visible-light photocatalysis. *Ceramics International, 39*(6), 7107-7113.
4. Wu, C., Yue, Y., Deng, X., Hua, W., & Gao, Z. (2004). Investigation on the synergetic effect between anatase and rutile nanoparticles in gas-phase photocatalytic oxidations. *Catalysis Today, 93*, 863-869.
5. Rajkumar, N., Mariammal, R. N., & Ramachandran, K. (2010). Synthesis and characterization of dye (Phenosafranine) sensitized flower-type ZnO nanorods. *International Journal of Modern Physics B, 24*(10), 1289-1298.
6. Janardhnan, S., & Sain, M. M. (2011). Targeted disruption of hydroxyl chemistry and crystallinity in natural fibers for the isolation of cellulose nano-fibers via enzymatic treatment. *BioResources, 6*(2), 1242-1250.
7. Khemiri, N., Abdelkader, D., Khalfallah, B., & Kanzari, M. (2013). Synthesis and characterization of CuIn2n+1S3n+2 (with n = 0, 1, 2, 3 and 5) powders.
8. Mehta, A. (2013). Ultraviolet-visible (UV-Vis) spectroscopy–Fieser-Kuhn rules to calculate wavelength of maximum absorption (Lambda-max) of polyenes (with sample problems).
9. Le, K. C. (2017). *73392 Thesis LE 2017*. https://doi.org/10.13140/RG.2.2.35396.27524
10. Akash, M. S. H., & Rehman, K. (2020). Ultraviolet-visible (UV-VIS) spectroscopy. In *Essentials of pharmaceutical analysis* (pp. 143-168). Springer.
11. Mandru, A., Mane, J., & Mandapati, R. (2023). A review on UV-visible spectroscopy. *Journal of Pharma Insights and Research, 1*(2), 91-96.
12. Skoog, D. A., Holler, F. J., & Crouch, S. R. (2007). *Principles of instrumental analysis* (6th ed.). Thomson Brooks/Cole.

13. Clark, J. (n.d.). UV-visible spectrometer. Chemguide. Retrieved from http://www.chemguide.co.uk/analysis/uvvisible/spectrometer.html
14. Kumar, V., & Singh, J. K. (2010). Model for calculating the refractive index of different materials.
15. Tsymbal, E. Y. (n.d.). *Introduction to solid state physics*. Physics 927.